Journal of Advanced Research in Numerical Heat Transfer

Journal homepage:
https://semarakilmu.com.my/journals/index.php/arnht/index
ISSN: 2735-0142

Laminar Mixed Convection Heat Transfer Analysis in Horizontal Annuli using Hybrid Nanofluid

Riyadh Fayez Sughayyir AlYasi[1], Nazrul Islam[1,*], Radi Abdulmonem Alsulami[1], Badr Ali Bzya Albeshri[2]

[1] Department of Mechanical Engineering, King Abdulaziz university, Jeddah-21589, Saudi Arabia
[2] Department of Mechanical Engineering, University of Hafr Al-Batin, KSA, Saudi Arabia

ARTICLE INFO

Article history:
Received 10 March 2023
Received in revised form 12 April 2023
Accepted 8 May 2023
Available online 30 June 2023

Keywords:
Mixed Convection; Hybrid Nanofluid; Concentric Annulus; Buoyancy Effect

ABSTRACT

Heat transfer can be augmented by employing different methodologies and techniques, such as increasing either the heat transfer surface or the heat transfer coefficient between fluid and surface that allows high heat transfer rates in a small volume. The enhanced thermal behavior of nanofluids could supply a basis for a huge innovation in heat transfer intensification. Recently, a new type of nanofluid, known as hybrid nanofluid, which consists of a mixture of two different nanoparticles suspended in the base fluid like water. The present study deals with the analysis of laminar mixed convection heat transfer in horizontal annuli using hybrid nanofluid with the thermal boundary condition of constant heat flux at the inner wall and isothermal outer wall. The SIMPLER numerical algorithm is adopted in the present study. The hybrid nanofluid consists of water as base fluid and Ag-TiO_2 as nanoparticles. The ratio of Ag to TiO_2 is maintained as 1:3. Main objective of the present study is to compute numerically three-dimensional axis-symmetric, incompressible, steady, laminar flow through annular ducts to investigate the effect of the hybrid nanofluid Ag-TiO_2/water on thermal-hydrodynamic characteristics. The analysis reveals that secondary flow due to the buoyancy forces plays an important role in augmenting heat transfer. The development of axial flow and temperature field are strongly found to be influenced by buoyancy. Nusselt number near the entrance region is found to be maximum, then attains a minimum value at a location slightly away from the entrance, and then starts increasing slowly due to the increased buoyancy effects. Finally, the flow becomes almost stable and a nearly constant value of Nusselt number is observed as the flow approaches fully development situation. At a given axial location Nusselt number was found to increase with increasing volumetric concentration of nanoparticle. The effect of Gr Radius ratio on the Nusselt number was also studied.

1. Introduction

To attain significant savings of cost and energy, intensification of heat transfer played a very indispensable role. Today's development in the field of science and technology is levitating the

* *Corresponding author.*
E-mail address: nabdulhafiz@kau.edu.sa (Nazrul Islam)

https://doi.org/10.37934/arnht.13.1.5265

demand for exceptionally featured compact devices with the best performance, accurate functioning, and long lifespan. Cooling is one of the most important technical challenges facing various diverse industries, including microelectronics. Therefore, a new improved performance for heat transfer is urgently needed. Superior thermal characteristics of hybrid nanofluids have not only declared it to be the most emerging heat transfer fluid but also the most fascinating one for future studies. Various geometries and thermal-hydraulic boundary conditions have been considered to study the enhancement of heat transfer. The present research problem involves laminar mixed convection heat transfer in horizontal annuli using a hybrid nanofluid.

The main objective of the present study is to compute numerically three-dimensional axis-symmetric incompressible, steady, laminar flow through annular ducts to investigate the effect of the hybrid nanofluid Ag-TiO_2/water on thermal-hydrodynamic characteristics for the thermal boundary condition of constant heat flux at the inner wall and isothermal outer wall. The effect of thermal boundary conditions, radius ratio, nanoparticle concentration, and Reynolds number on Nusselt number and friction factor will also be studied for these flow conditions.

Heat transfer can be enhanced by employing different methodologies and techniques, such as increasing the heat transfer surface or the heat transfer coefficient between fluid and surface, allowing high heat transfer rates in a small volume. The enhanced thermal behaviour of nanofluids could supply a basis for a massive innovation in heat transfer intensification. This technology is essential to several industrial sectors, including manufacturing, transportation, power generation, micro-manufacturing, solid-state lighting, thermal therapy for cancer treatment, chemical and metallurgical sectors, heating, cooling, ventilation, and air-conditioning. Cooling is one of the most critical technical challenges facing various industries, including microelectronics. Therefore, a new, improved performance for heat transfer is urgently needed. Superior thermal characteristics of hybrid nanofluids have declared it to be the most emerging heat transfer fluid and the most fascinating one for future studies. Instead of that, today, investigators are not in a position to exercise the hybrid nanofluids in domestic or industrial applications due to many problems that need to be resolved. However, researchers worldwide have taken this responsibility and devoted their abilities, but they are very few.

Recently, Benkhedda *et al.,* [1] have carried out a numerical investigation of laminar mixed convection in horizontal annulus filled with a TiO_2/water nanofluid and Ag TiO_2/water hybrid nanofluid with outer cylinder uniformly heated while the inner cylinder is adiabatic. Benkhedda *et al.,* [1] have concluded that the use of the hybrid nanofluid led to an increase in the heat transfer concerning the use of the nanofluid or the base fluid. They recommended that experimental and numerical studies should be intensified to deepen the understanding of the behaviour of this new type of fluid in the fields of fluid dynamics or rheology and heat transfer field. This knowledge will undoubtedly lead to a clear improvement in the heat transfer within the hybrid nanofluid and in contact with a wall and eventually, open the way to the diversification of the fields of application in the industry.

Following this rich evolution of the nanofluid field, the present work has been intended to perform the numerical simulation of a specific hybrid nanofluid, Ag-TiO2/water, with the thermal boundary condition of constant heat flux at the inner wall and isothermal outer wall [1].

From the analysis of the available literature, it appears that most of the studies are relevant to Newtonian fluids, constant thermophysical properties, stationary bounding surfaces, and uniform thermal boundary conditions [2-12]. Only a delimited number of authors have considered different needs such as constant heat flux along the periphery of the inner cylinder, forced convection due to a cooled rotating outer cylinder, temperature-dependent viscosity, thermo dependent non-Newtonian fluids, and non-uniform circumferential heating [13-18]. Finally, Chenier *et al.,* [19]

performed numerically a linear stability investigation of a fully developed mixed convection flow of air in an annular horizontal vent.

2. Numerical Methodology

The physical model considered in the present study is shown in Figure 1 The inner wall of the annulus is maintained at a uniform heat flux, while the outer wall is isotherm.

Due to the concentric annular geometry of the problem a cylindrical coordinate system, as shown in Figure 1, has been chosen. Following assumptions are made for the formulation of the problem,

i. the flow is laminar and steady
ii. the fluid is incompressible with density variation taken into account only in the body force terms.
iii. the flow is assumed to be symmetric across the vertical plane (θ=0°, θ= 180°) passing through the axis of the annulus.

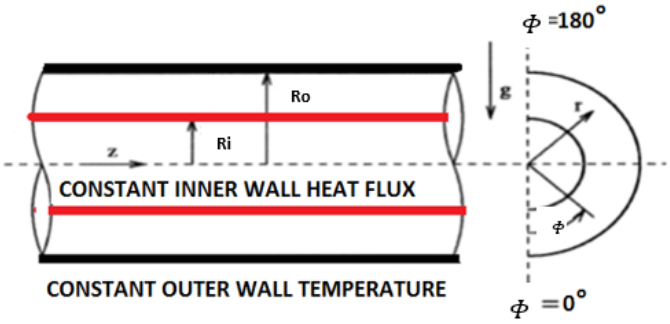

Fig. 1. Schematic diagram of the flow situation

The problem is analysed for constant fluid properties. The variation of density is taken into account only in the body forces (Boussinesq approximation). The body force term in the radial momentum equation is

$$\rho g_r = \rho g \cos \Phi \tag{1}$$

Where Φ is measured as shown in Figure 1 the density ρ is given by:

$$\rho = \rho_i [1 - \beta (T - T_i)] \tag{2}$$

Eq. (6) can be expressed as:

$$\rho g_r = \rho_i [1 - \beta (T - T_i)] \cos \Phi \tag{3}$$

The body force term in the Φ-direction momentum equation can be similarly written as:

$$\rho g_\Phi = -\rho_i g [1 - \beta (T - T_i)] \, sin \, \Phi \tag{4}$$

With the assumptions mentioned, the set of governing equations can be simplified as follows:

Continuity equation (conservation of mass):

$$\frac{1}{r}\frac{\partial}{\partial r}(r\,v)+\frac{1}{r}\frac{\partial w}{\partial \Phi}+\frac{\partial u}{\partial z}=0 \tag{5}$$

Conservation of momentum in the radial direction:

$$\frac{1}{\mathrm{r}}\frac{\partial}{\partial \mathrm{r}}\left[(\rho\,\mathrm{v}\,\mathrm{r})\mathrm{v}-\mu\,\mathrm{r}\frac{\partial \mathrm{v}}{\partial \mathrm{r}}\right]+\frac{1}{\mathrm{r}}\frac{\partial}{\partial \Phi}\left[\rho\,\mathrm{w}\,\mathrm{v}\;-\frac{\mu}{\mathrm{r}}\frac{\partial \mathrm{v}}{\partial \Phi}\right]+\frac{\partial}{\partial \mathrm{z}}\left[\rho\mathrm{U}\mathrm{v}-\;\mu\frac{\partial \mathrm{v}}{\partial \mathrm{z}}\right]=\;-\frac{\partial \mathrm{pc}}{\partial \mathrm{r}}+\rho\mathrm{g}\beta\,(\mathrm{T}-\mathrm{Ti})\cos\Phi+\frac{\rho w^2}{\mathrm{r}}-\frac{2\mu}{\mathrm{r}^2}\frac{\partial \mathrm{w}}{\partial \Phi}-\frac{\mu \mathrm{w}}{\mathrm{r}^2} \tag{6}$$

Conservation of momentum in the tangential direction:

$$\frac{1}{\mathrm{r}}\frac{\partial}{\partial \mathrm{r}}\left[(\rho\,\mathrm{v}\,\mathrm{r})\mathrm{w}-\mu\,\mathrm{r}\frac{\partial \mathrm{w}}{\partial \mathrm{r}}\right]+\frac{1}{\mathrm{r}}\frac{\partial}{\partial \Phi}\left[\rho\,w\,w-\frac{\mu}{\mathrm{r}}\frac{\partial \mathrm{w}}{\partial \Phi}\right]+\frac{\partial}{\partial \mathrm{z}}\left[\rho\mathrm{U}\mathrm{w}-\;\mu\frac{\partial \mathrm{w}}{\partial \mathrm{z}}\right]=\;-\frac{1}{\mathrm{r}}\frac{\partial \mathrm{pc}}{\partial \Phi}+\rho\mathrm{g}\beta\,(\mathrm{T}-\mathrm{Ti})\sin\Phi+\frac{\rho \mathrm{v}\mathrm{w}}{\mathrm{r}}-\frac{2\mu}{\mathrm{r}^2}\frac{\partial \mathrm{v}}{\partial \Phi}-\frac{\mu \mathrm{w}}{\mathrm{r}^2} \tag{7}$$

Conservation of momentum in the axial direction:

$$\frac{1}{r}\frac{\partial}{\partial r}\left[(\rho\,v\,r)u-\mu\,r\frac{\partial u}{\partial r}\right]+\frac{1}{r}\frac{\partial}{\partial \Phi}\left[\rho\,w\,u-\frac{\mu}{r}\frac{\partial u}{\partial \Phi}\right]+\frac{\partial}{\partial z}[\rho\,u\,u]=\;-\;\frac{\partial p}{\partial z} \tag{8}$$

Conservation of energy:

$$\frac{1}{r}\frac{\partial}{\partial \mathrm{r}}\left[(\rho\,\mathrm{v}\,)\mathrm{Cp}\;\mathrm{T}-\;\mathrm{rk}\;\frac{\partial \mathrm{T}}{\partial \mathrm{r}}\right]+\frac{1}{\mathrm{r}}\frac{\partial}{\partial \Phi}\left[\rho\,\mathrm{w}\,\mathrm{Cp}\;\mathrm{T}-\frac{\mathrm{k}}{\mathrm{r}}\frac{\partial \mathrm{T}}{\partial \Phi}\right]\frac{\partial}{\partial \mathrm{z}}[\rho\mathrm{U}\mathrm{Cp}\;\mathrm{T}\,]=\;0 \tag{9}$$

The set of governing Eq. (8) and Eq. (9) must be solved simultaneously for simulating combined free and force convection phenomenon in horizontal concentric cylindrical annulus according to the specified boundary condition. In these equations, the fluid density at the inlet, ρ_i has been denoted by ρ. The following boundary conditions are imposed while solving the governing equations:

i. Symmetry lines ($R_i < R < R_o\;;\;\Phi = 0\;or\;\pi$): $w = 0, \frac{\partial v}{\partial \Phi} = 0\;and\;\frac{\partial T}{\partial \Phi} = 0$
ii. Inner cylinder ($R = R_i\;;0\;< \Phi < \pi$): $v = w = u = 0, and - k\frac{\partial T}{\partial r} = q$
iii. Outer cylinder ($R = R_o\;;0 < \Phi < \pi$): $v = w = 0 = u = 0,\;\;and\;T = T_{ow}$
iv. Inlet (z=0): $v = w = 0, u = ui\;\;and\;T = T_i$

Thermo physical properties of TiO2-water nanofluid are defined as follows:

The density of the nanofluid is given by:

$$\rho_{nf} = \psi\rho_p + (1-\psi)\rho_f \tag{10}$$

The nanofluid heat capacitance is expressed as:

$$(\rho C_p)_{nf} = \psi(\rho C_p)_p + (1-\psi)\left(\rho C_p\right)_f \tag{11}$$

The thermal expansion coefficient of the nanofluid can be determined by:

$$(\rho\beta)_{nf} = \psi(\rho\beta)_p + (1-\psi)(\rho\beta)_f \tag{12}$$

where n is an empirical shape factor given by n = 3/α (α is the particle sphericity definite as the ratio amongst the surface area of the sphere and the surface area of the factual particle with identical volume).

The viscosity of the nanofluid as:

$$\mu_{nf} = \frac{\mu_f}{(1-\psi)^{2.5}} \tag{13}$$

Thermophysical properties of TiO2-Ag-water hybrid nanofluid are as follow:

The density is specified by:

$$\rho_{hnf} = \psi_{Tio_2}\rho_{Tio_2} + \psi_{Ag}\rho_{Ag} + (1-\psi)\rho_f \tag{14}$$

ψ considered as the overall volume concentration of two dissimilar types of nanoparticles disseminated in hybrid nanofluid and is considered as:

$$\psi = \psi_{Tio_2} + \psi_{Ag} \tag{15}$$

The heat capacitance:

$$(\rho C_p)_{hnf} = \psi_{Tio_2}\rho_{Tio_2}C_{p_{Tio_2}} + \psi_{Ag}\rho_{Ag}C_{p_{Ag}} + (1-\psi)(\rho C_p)_f \tag{16}$$

The thermal conductivity coefficient is determined by:

$$\frac{k_{hnf}}{k_f} = \frac{(k_{hp}+2k_f)-2\psi(k_f-k_{hp})}{(k_{hp}+2k_f)+2\psi(k_f-k_{hp})} \quad \text{where} \quad k_{hp} = \frac{\psi_{Tio_2}k_{Tio_2}+\psi_{Ag}k_{Ag}}{\psi} \tag{17}$$

The subscript hp stands for hybrid nanoparticles. The governing equations are discretized according to the finite difference method. The present problem has been formulated using a hybrid scheme [20]. After discretization, these equations have been solved simultaneously by following a sequence of steps. SIMPLER algorithm has been adopted in the present work [20]. The 3-D mesh of the computational domain is shown in Figure 2. A typical finite volume of dimension ΔV= r Δr Δ Φ Δz, as shown in Figure 3, is characterized by a node P at the center and six interfaces adjacent to the neighboring nodes in the radial (N and S), angular (W and E) and axial (T and B) directions. All the scalar quantities are stored at the node P, while the vector quantities are crossing through the centre of the six faces, n, s, e, w, b and t, surrounding each control volume. The length of the annulus is 1000 mm. To keep the program simple, uniform grids were used in the r- Φ coordinates. The effect of grid sizes (Δr x Δ Φ x Δz) on the axial (Z_{nd}=z/Dh) variation of Nusselt number is shown in Figure 4. The axial length is denoted by z and Nusselt number, Nu, is defined as

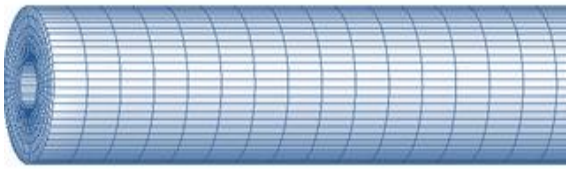

Fig. 2. 3-D mesh of the computational domain

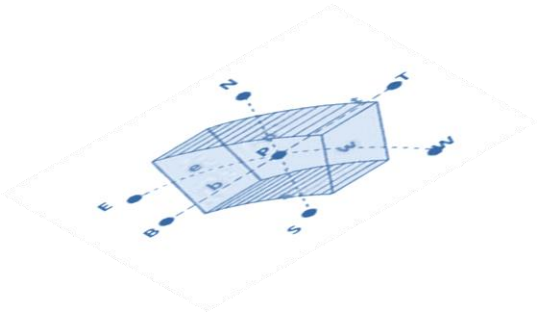

Fig. 3. Typical grid geometry

$$Nu = \frac{h\, D_h}{k} \tag{18}$$

where h is coefficient of convective heat transfer. To check the grid independence, the results were obtained for radius ratio, R = 2, Reynolds number, Re = 600, Grashoff number, Gr = 6x10^{5}and ψ = 0.0, using five sets of grids: (i) 20x20, (ii) 28x28, (iii) 36x36, (iv) 44x44 and (v) 52x52 grids in the r-Φ plane. Re and Gr are defined as:

$$Re = \frac{\rho V D_h}{\mu} \tag{19}$$

$$Gr = \frac{g\, \beta\, D_h^4\, q}{v^2\, k} \tag{20}$$

where v is the kinematic viscosity and q is the wall heat flux. Based on the grid independence test results, as shown in Figure 4 and Figure 5, a 48x48 grid in the r-Φ plane has been chosen because 52x52 and 44x44 grid in the r-Φ plane is very identical, so we can choose any grid between them, with the number of grids in the axial direction equal to 4000. Hence, for a uniform mesh for an axial length of 1.0 m, Δz=0.25 mm.

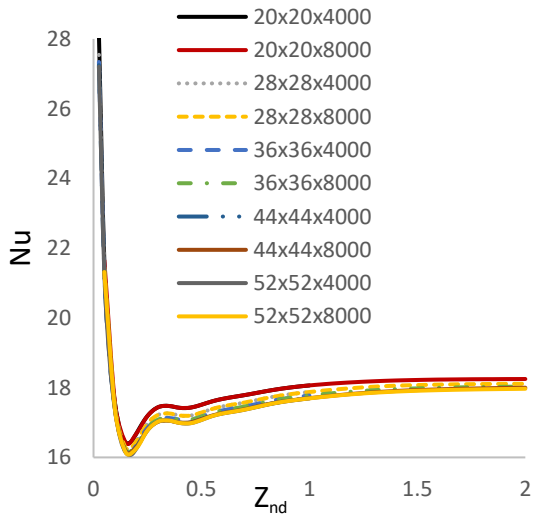

Fig. 4. Effect of different grid sizes (r-Φ-Δz) on axial Nusselt number for Re=600, Gr=6x10^5 and ψ =0

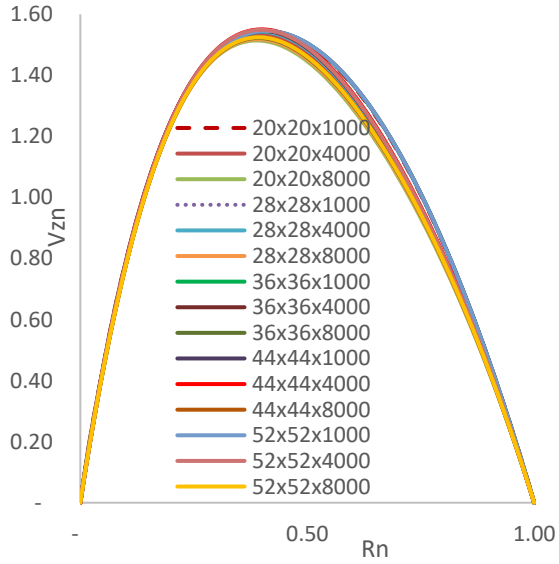

Fig. 5. Effect of grid sizes on axial velocity profile for Re=600, Gr=6x10^5 and ψ=0

3. Results

The isotherms at a cross section deviate from the circular shape when buoyancy effects become impressive. Figure 6 shows the development of isotherms for Gr=10^6, RR=2, Re=600, and ψ=0.05. At the entrance, Z_{nd}=2.5 [Figure 6(a)] the isotherms are almost circular and are unaffected by the flow, and most of the fluid is still at the inlet temperature. When the fluid moves from the entrance, the buoyancy forces become more powerful and start affecting the temperature field. At Z_{nd}=10 [Figure 6(b)], it is observed that the isotherms at the lower part of the cross section are still nearly circular, indicating weak secondary motion in this region. The stronger buoyancy effect in the upper half of the cross section, however, causes noticeable distortion in the temperature field. The isotherms at this location have a tendency to become horizontal, approximating the temperature distribution to a stable stratified field. Further downstream, from Z_{nd}=50 [Figure 6(d)] to Z_{nd}=100 [Figure 6(e)], more thermal stratification takes place, and consequently, the buoyancy forces become stable.

The effect of flow development on the radial velocity component for Gr=10^6, RR=2, Re=600, and ψ=0.05 is shown in Figure 7. Since, a flat velocity profile is supposed at the entrance, the radial velocity must be zero at this location. Near the entrance, at Z_{nd}=2.5 [Figure 7(a)], the distortion in the radial isovels is seen to be small, hence, the effect of buoyancy caused by flow is insignificant in this region. When the fluid moves from the entrance, the buoyancy forces become more powerful and start affecting the radial velocity. It can be seen that there are two distinct areas of flow, radial velocity positive in the upper area of the annulus while in the lower area the radial velocities are negative. Positive radial velocity occurrence in the upper part of the annulus may be attributed to the more powerful buoyancy effect in that region as clear from the corresponding isotherms in Figure 6. At Z_{nd}=10 [Figure 7 (b)], a location more away from the inlet, the positive velocity area is seen to be toward the upper part of the annulus. Also, the emergence of secondary velocity is observed. As the flow develops, at Z_{nd}=25 [Figure 7(e)], positive radial velocities are seen to be mostly concentrated in the upper part of the annulus owing to the stability of the flow.

The development of dimensionless axial is ovels (V_{zn}) present is presented in Figure 8 for Gr=10^6, RR=2, Re=600, and ψ =0.05. The buoyancy-induced secondary flow tends to distort the axial velocity profiles. At Z_{nd}=2.5, [Figure 8(a)], a location near the entrance, due to weaken buoyancy effects, as is clear from the isotherms in [Figure 6(a)], the axial isovels are circular in shape that resembles the axial isovels for pure forced convection. As the fluid moves away from the inlet, the axial is ovels start deviating from the corresponding axial is ovels for pure forced convection. It is seen in [Figure 8(b)] (Z_{nd}=10) that the axial velocities in the top region of the cross section are highly distorted due to the stronger buoyancy effect in this region, whereas little distortion is noticed in the bottom region. This results in ununiform distribution of mass flux, the minimum being at the top and the maximum at the bottom. Further downstream (Z_{nd}≥25), the is ovels have a tendency for attaining the fully developed situation.

The effect of flow development on the tangential component of velocity for Gr=10^6, RR=2, Re=600, and ψ =0.05 is shown in Figure 9. Since a flat velocity profile is assumed at the entrance, the angular velocity must be zero at this location. However, due to the effect of free convection, even near the entrance, at Z_{nd}=2.5 [Figure 9(a)], emergence of angular velocities is observed. It is seen that the angular velocities are positive near the inner wall and negative near the outer wall. It is also noticed that near the entrance the magnitudes of the angular velocities are small. However, as the flow develops (Z_{nd} ≥10), due to more powerful buoyancy effect the magnitude of the angular velocities are increasing.

Figure 10 presents the effect of flow development and different angles on the fluid temperature along the radial direction for Re=600 and Gr=10^6 is shown in Figure 10 the fluid temperature near the

inner wall is maximum and then starts decreasing becomes zero which indicates that no effect of inner wall heating beyond Rn=0.2. Since the outer wall is isothermal, most part of the annulus is unaffected by temperature change. However, with the development of flow and effect of angles, the magnitude of the temperature increases. Figure 11 presents the effect of flow development and dimensionless radial coordinate on the variation of bulk fluid temperature along angular direction for Re=600 and $Gr=10^6$. It is seen in the figure that in the lower half of the annulus, the dimensionless temperatures are constant and of very small magnitudes. However, in the upper half of the annulus, the temperatures are seen to be of higher magnitudes due to stronger buoyancy effect there. This behaviour is also clear from the isotherms of Figure 6.

Figure 12 presents the effect of the flow development and different dimensionless radial coordinate on the variation of radial velocity along the angular direction. As seen in the figure, near the entrance (Z_{nd} = 2.5), the radial velocity is almost zero in the lower half ($\Phi \leq 90^o$) of the annulus and is positive and very small in magnitude in the upper half ($\Phi \geq 90^o$) of the annulus. At Z_{nd} = 10, a location slightly away from the entrance, the effect of free convection is still insignificant as clear from the isotherms in Figure 6. As the flow develops ($Z_{nd} \geq 25$), the radial velocities are highly affected at the upper half ($\Phi \leq 90^o$) of the annulus, whereas the radial velocities in the lower half ($\Phi \geq 90^o$) of the annulus is almost unchanged.

The effect of flow development in terms of axial velocity profile along radial direction for Re=600 and $Gr=10^6$ is presented in Figure 13 Near the entrance (Z_{nd}=2.5) the axial velocity profile is of semi-flat type indicating inception of flow development. As the flow develops ($Z_{nd}\geq10$) the location of maximum axial velocity shifts towards the inner wall. This may be attributed to the effect of stronger buoyancy forces near the inner wall which is at constant heat flux. Figure 14 presents the Effect of flow development on the variation of Axial velocity along angular direction for Re=600 and $Gr=10^6$. It can we be seen in the figure that near the entrance (Z_{nd}=2.5), the axial velocity is constant along the angular direction. However, as the flow develops, the axial velocities in the upper half ($\Phi \geq 90^o$) of the annulus decrease owing to the stronger buoyancy effect in that region as clear from the isotherms of Figure 6.

Figure 15 shows the effect of flow development on the variation of angular velocity along the radial Rn= [(R–Ri) / (Ro–Ri)] direction. Near the inlet location at Z_{nd} = 2.5 of the annuli, the angular velocity near the inner wall ($0\leq Rn\leq 0.2$) first increases along the radial length and then starts decreasing and finally reverses its direction from positive to negative and remains almost constant in the remaining portion ($0.2 \leq Rn \leq 1.0$) of the annulus. This can well be understood from the isotherms of Figure 6 as the magnitude of isotherms away from the inner wall is very small. As the flow develops ($Z_{nd} \geq 10$), the radial velocities are seen to be increasing owing to the effect stronger buoyancy effect. It is observed that with the development of flow, the distribution of the positive velocities is increasing near the inner wall. This distribution is about 40% for the case of Z_{nd} = 100. The effect of flow development in terms of axial velocity profile along the tangential direction is presented in Figure 13. Near the entrance (Z_{nd} = 2.5) the axial velocity profile is of semi-flat type indicating inception of flow development. As the flow develops ($Z_{nd} \geq 10$) the location of maximum axial velocity shifts towards the inner wall. This may be attributed to the effect of stronger buoyancy forces near the inner wall, which is a constant heat flux, as depicted from Figure 6.

Figure 16 shows the effect of volumetric concentration, Nusselt number increase with increasing volumetric concentration. Nusselt number is also seen to increase with increasing radius ratio as shown in Figure 17.

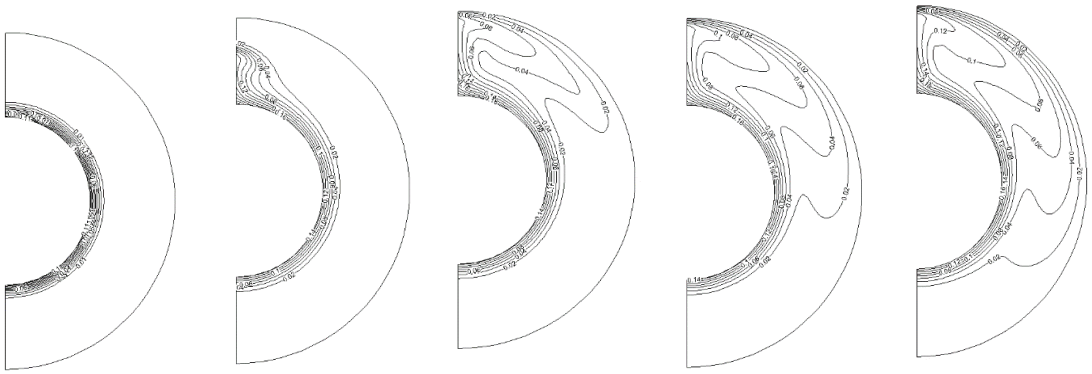

(a) Z_{nd}=2.5 (b) Z_{nd}=10 (c) Z_{nd}=25 (d) Z_{nd}=50 (e)Z_{nd}=100

Fig. 6. Development of isotherms for Re=600 and Gr=E6 and ψ =0.05

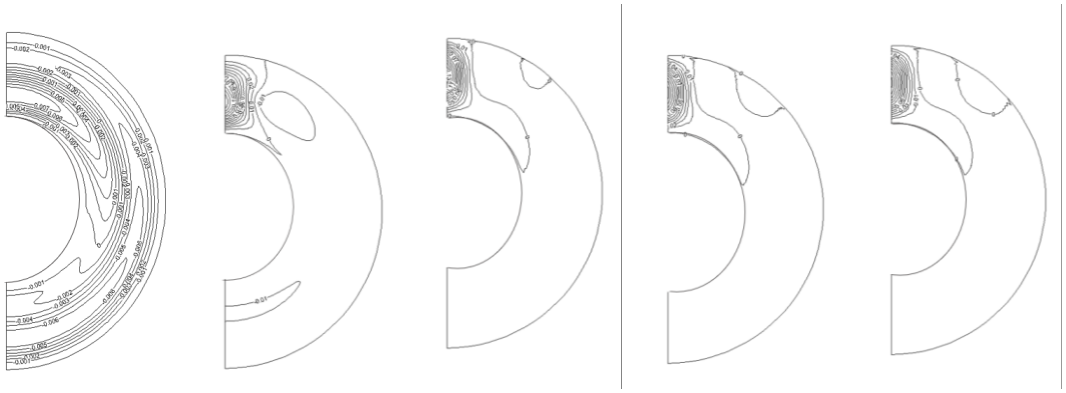

(a) Z_{nd}=2.5 (b) Z_{nd}=10 (c) Z_{nd}=25 (d) Z_{nd}=50 (e) Z_{nd}=100

Fig. 7. Development radial velocity for Re=600 and Gr=E6 and ψ =0.05

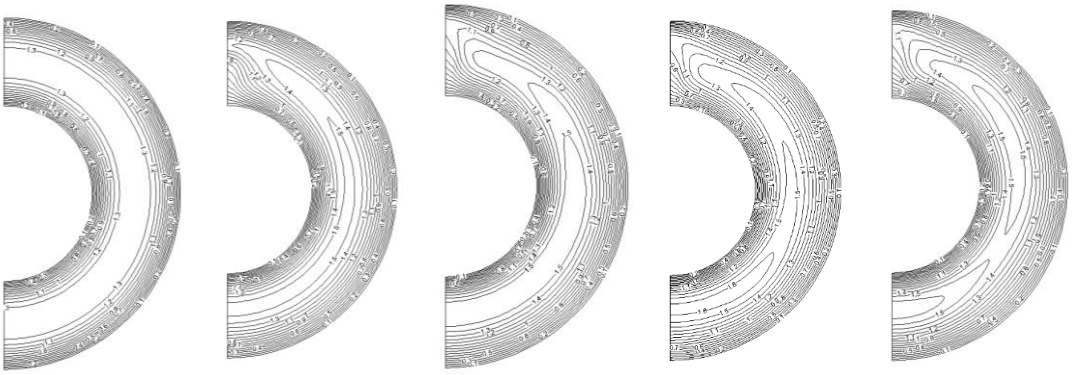

(a) Z_{nd}=2.5 (b) Z_{nd}=10 (c)Z_{nd}=25 (d) Z_{nd}=50 (e) Z_{nd}=100

Fig. 8. Development of axial velocity for Re=600 and Gr=E6 and ψ =0.05

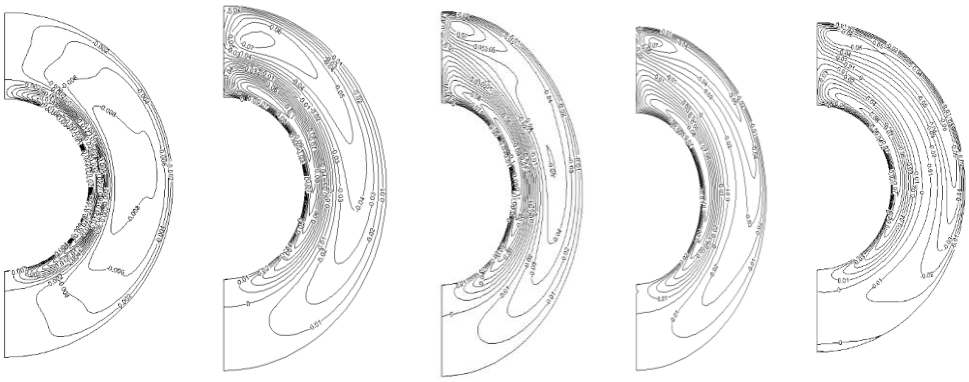

(a) Z_{nd}=2.5 (b) Z_{nd}=10 (c) Z_{nd}=25 (d) Z_{nd}=50 (e) Z_{nd}=100

Fig. 9. Development of tangential velocity for Re=600 and Gr=E6 and ψ =0.05

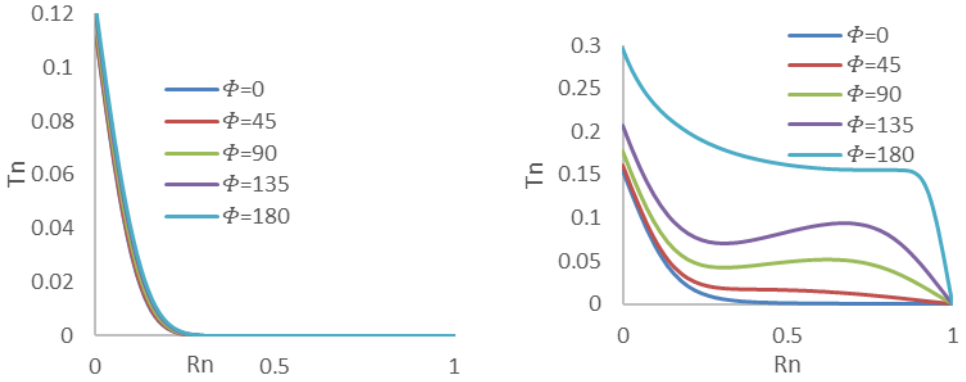

Fig. 10. Effect of flow development and different angels on the variation of dimensionless temperature (T_n) along radial direction for Re=600, Gr=E6 and ψ=0.05

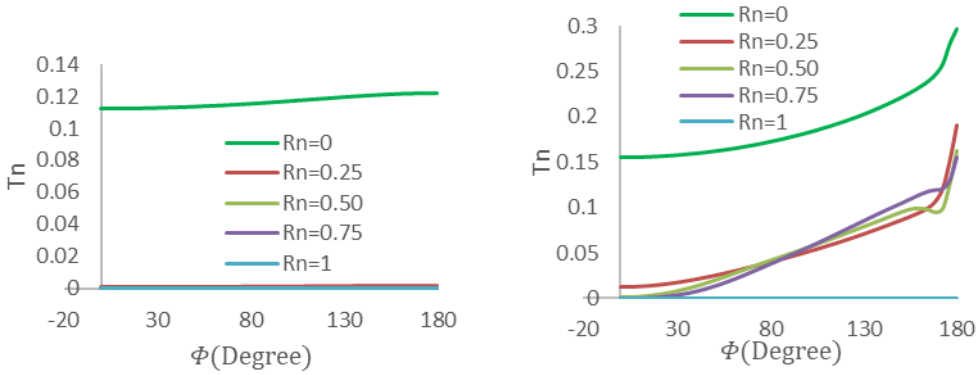

Fig. 11. Effect of flow development and different daimesionless radial coordinate on the variation of dimentionless temperature (T_n) along angular direction for Re=600 , Gr=E6 and ψ=0.05

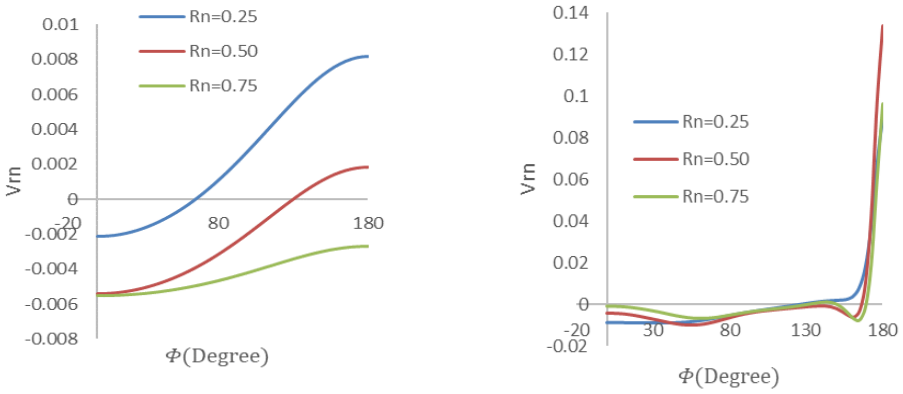

(a) Z_{nd}=2.5 (b) Z_{nd}=100

Fig. 12. Effect of flow development and different dimensionless radial coordinate on the variation of dimensionless radial velocity (V_{rn}) along the angular direction for Re=600, Gr=E6 and ψ=0.05

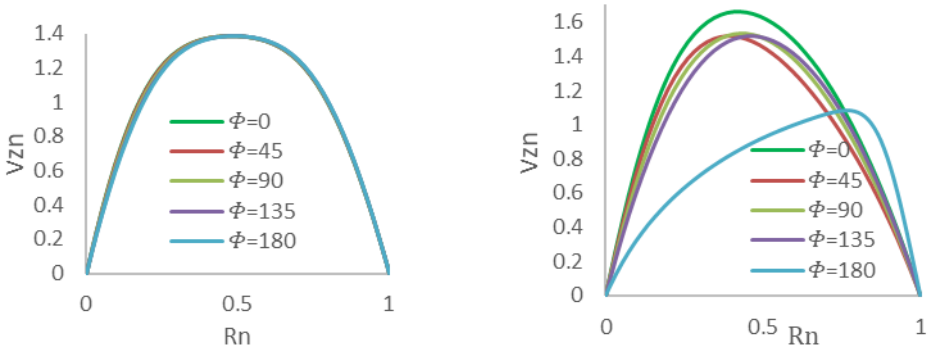

(a) Z_{nd}=2.5 (b) Z_{nd}=100

Fig. 13. Effect of flow development and different angels on the variation of dimensionless axial velocity (V_{zn}) along the angular direction for Re=600, Gr=E6 and ψ=0.05

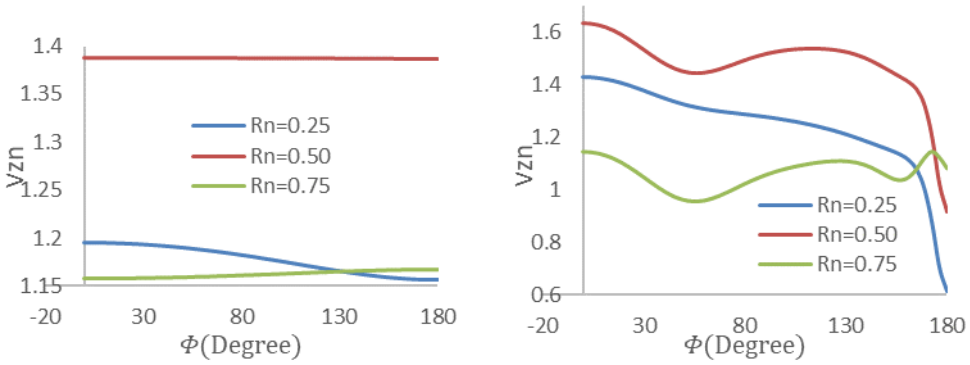

(a) Z_{nd}=2.5 (b) Z_{nd}=100

Fig. 14. Effect of flow development and different dimensionless radial coordinate on the variation of dimensionless axial velocity (V_{zn}) along the angular direction for Re=600, Gr=E6 and ψ=0.05

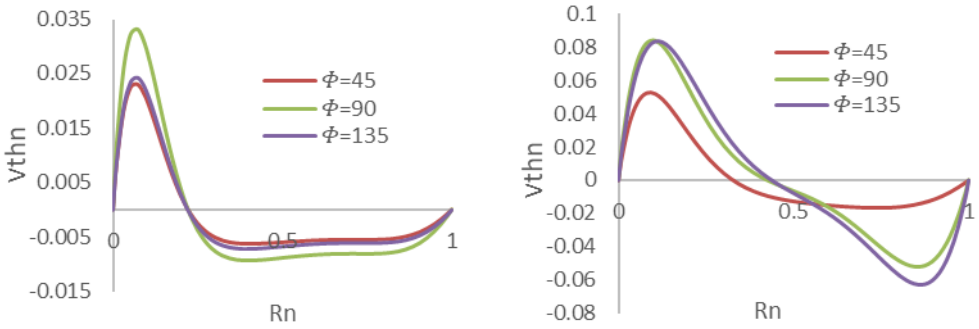

(a) Z_{nd}=2.5 (b) Z_{nd}=100

Fig. 15. Effect of flow development and different angles on the variation of dimensionless angular velocity (V_{thn}) along the angular direction for Re=600, Gr=E6 and ψ=0.05

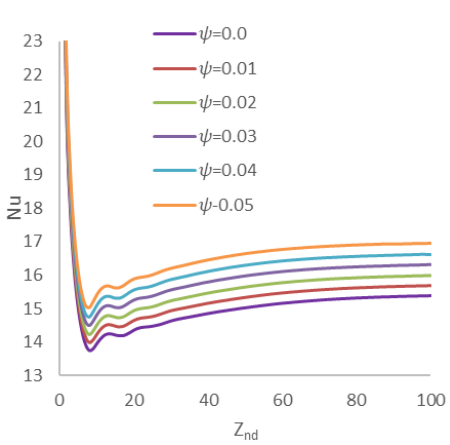

Fig. 16. Effect of volumetric concentration on Nusselt number for RR=2, Re=600, Gr=E6

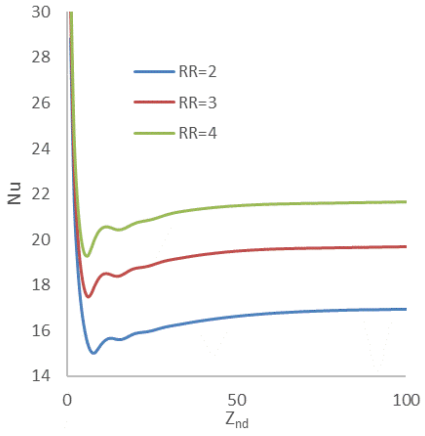

Fig. 17. Effect of radius ratio on Nusselt number for Re=600, Gr=E6, ψ=0.05

4. Conclusions

In the present work, analyses have been carried out to study the heat transfer and fluid flow characteristics of a hybrid nanofluid with Ag-TiO_2 nanoparticles dispersed in water for mixed convection situation in the entrance region of the horizontal concentric annulus with thermal boundary condition of inner wall at constant heat flux and outer wall being isothermal. The investigation reveals that the effect of secondary flow due to the buoyancy forces is stronger in the upper half of the annular cross-section. It increases throughout the cross-section until its intensity reaches a maximum, and then it becomes weak far downstream. The development of axial flow and temperature field is strongly influenced by the buoyancy induced secondary flow. The buoyancy influence is stronger near the inlet section where it is characterized by a deceleration of the axial flow in the upper part of the annulus and an acceleration of the axial flow in the lower part of the annulus. Also, it appears that the Nusselt number increasing with increasing in radius ratio and volumetric concentration.

Acknowledgement
This research was not funded by any grant.

References
[1] Benkhedda, Mohamed, Toufik Boufendi, and S. Touahri. "Laminar mixed convective heat transfer enhancement by using Ag-TiO 2-water hybrid Nanofluid in a heated horizontal annulus." *Heat and Mass Transfer* 54 (2018): 2799-2814. https://doi.org/10.1007/s00231-018-2302-x

[2] N. Hattori. "Combined free and forced convection heat transfer for fully developed laminar flow in concentric annuli, numerical analysis." *Trans. JSME* (1979): 227-239. https://doi.org/10.1299/kikaib.45.227

[3] Mojtabi, Abdelkader, and J-P. Caltagirone. "Analyse du transfert de chaleur en convection mixte laminaire entre deux cylindres coaxiaux horizontaux." *International Journal of Heat and Mass Transfer* 23, no. 10 (1980): 1369-1375. https://doi.org/10.1016/0017-9310(80)90211-2

[4] Nguyen, T. Hung, P. Vasseur, L. Robillard, and B. Chandra Shekar. "Combined free and forced convection of water between horizontal concentric cylinders." (1983): 498-504. https://doi.org/10.1115/1.3245613

[5] Kotake, S., and N. Hattori. "Combined forced and free convection heat transfer for fully-developed laminar flow in horizontal annuli." *International journal of heat and mass transfer* 28, no. 11 (1985): 2113-2120. https://doi.org/10.1016/0017-9310(85)90105-X

[6] Nieckele, A. O., and S. V. Patankar. "Laminar mixed convection in a concentric annulus with horizontal axis." (1985): 902-909. https://doi.org/10.1115/1.3247519

[7] Kaviany, M. "Laminar combined convection in a horizontal annulus subject to constant heat flux inner wall and adiabatic outer wall." (1986): 392-397. https://doi.org/10.1115/1.3246935

[8] Ciampi, M., Sergio Faggiani, Walter Grassi, Frank P. Incropera, and G. Tuoni. "Experimental study of mixed convection in horizontal annuli for low Reynolds numbers." In *International Heat Transfer Conference Digital Library*. Begel House Inc., 1986. https://doi.org/10.1615/IHTC8.2910

[9] Karki, Kailash C., and Suhas V. Patankar. "Laminar mixed convection in the entrance region of a horizontal annulus." *Numerical heat transfer* 15, no. 1 (1989): 87-99. https://doi.org/10.1080/10407788908944678

[10] Nonino, Carlo, and Stefano Del Giudice. "Finite element analysis of laminar mixed convection in the entrance region of horizontal annular ducts." *Numerical Heat Transfer, Part A Applications* 29, no. 3 (1996): 313-330. https://doi.org/10.1080/10407789608913795

[11] Islam, Nazrul, Uday N. Gaitonde, and G. K. Sharma. "Combined free and forced convection heat transfer in a horizontal annulus." In *International Heat Transfer Conference Digital Library*. Begel House Inc., 1998. https://doi.org/10.1615/IHTC11.3210

[12] Mohammed, Hussein A., Antonio Campo, and Rahman Saidur. "Experimental study of forced and free convective heat transfer in the thermal entry region of horizontal concentric annuli." *International Communications in Heat and Mass Transfer* 37, no. 7 (2010): 739-747. https://doi.org/10.1016/j.icheatmasstransfer.2010.04.007

[13] Islam, Nazrul, U. N. Gaitonde, and G. K. Sharma. "Mixed convection heat transfer in the entrance region of horizontal annuli." *International journal of heat and mass transfer* 44, no. 11 (2001): 2107-2120. https://doi.org/10.1016/S0017-9310(00)00223-4

[14] Albeshri, Badr Ali Bzya, Nazrul Islam, Ahmad Yahya Bokhary, and Amjad Ali Pasha. "Hydrodynamic Analysis of Laminar Mixed Convective Flow of Ag-TiO2-Water Hybrid Nanofluid in a Horizontal Annulus." *CFD Letters* 13, no. 7 (2021): 47-57. https://doi.org/10.37934/cfdl.13.7.4557

[15] Yoo, Joo-Sik. "Mixed convection of air between two horizontal concentric cylinders with a cooled rotating outer cylinder." *International journal of heat and mass transfer* 41, no. 2 (1998): 293-302. https://doi.org/10.1016/S0017-9310(97)00141-5

[16] Nouar, C. "Numerical solution for laminar mixed convection in a horizontal annular duct: Temperature-dependent viscosity effect." *International journal for numerical methods in fluids* 29, no. 7 (1999): 849-864. https://doi.org/10.1002/(SICI)1097-0363(19990415)29:7<849::AID-FLD820>3.0.CO;2-F

[17] Nouar, Chérif, Braham Benaouda-Zouaoui, and Christophe Desaubry. "Laminar mixed convection in a horizontal annular duct. Case of thermodependent non-Newtonian fluid." *European Journal of Mechanics-B/Fluids* 19, no. 3 (2000): 423-452. https://doi.org/10.1016/S0997-7546(00)00120-5

[18] Habib, M. A., and A. A. A. Negm. "Laminar mixed convection in horizontal concentric annuli with non-uniform circumferential heating." *Heat and Mass Transfer* 37, no. 4-5 (2001): 427-435. https://doi.org/10.1007/s002310000153

[19] Chénier, Eric, G. Petrone, and Guy Lauriat. "From natural to mixed convection in horizontal and differentially heated annular ducts: Linear stability analysis." *International journal of heat and mass transfer* 54, no. 23-24 (2011): 5100-5108. https://doi.org/10.1016/j.ijheatmasstransfer.2011.07.028

[20] Patankar, Suhas. *Numerical heat transfer and fluid flow*. Taylor & Francis, 2018. https://doi.org/10.1201/9781482234213